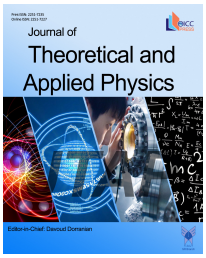

Volume 18, Issue 4, 182451 (1-10)

Journal of Theoretical and Applied Physics (JTAP)

https://dx.doi.org/10.57647/j.jtap.2024.1804.51

One-dimensional study of spatiotemporal evolution of magnetic field by Weibel instability in counter-streaming plasma flows

Rakesh Kumar[1], Hitendra K. Malik[1,*], Sandeep Kumar[2]

[1]*Plasma Waves and Particle Acceleration Laboratory, Department of Physics, Indian Institute of Technology Delhi, New Delhi, India.*
[2]*Department of Physics, Manav Rachna University, Faridabad, India.*

[*]**Corresponding author:** hkmalik@physics.iitd.ac.in

Original Research

Received:
7 May 2024
Revised:
27 June 2024
Accepted:
8 July 2024
Published online:
30 August 2024

Abstract:

The plasma filamentation instability (FI), also known as the beam-Weibel instability, is responsible for the generation of magnetic fields and the acceleration of particles within collisionless astrophysical plasmas. In the present study, we employ Particle-In-Cell (PIC) simulation to model the filamentation instability driven by sub-relativistic electron-positron counter-streaming pairs in one spatial dimension moving with velocity $v = \pm 0.5c\hat{x}$. The temperature is taken to be hotter in one direction. The simulation box is aligned in y-direction (perpendicular to the beam velocity vector) with normalized length 120 c/ω_{pe}. The magnetic field is found to grow unconstrainedly and causes the particles to reorganize in space. Our findings have revealed that the magnetic pressure gradient that forms during the quasilinear evolution of the filamentation instability results in generating an electrostatic field component and both the electrostatic field and the magnetic field act to redistribute the particles within the spatial domain. The electromagnetic fields lead to the thermalization of the electrons. The filamentation instability exhibits effective mechanisms for accelerating electrons to high energy levels.

Keywords: Counter-streaming electron-positron plasma flow; Pair-plasma; Weibel instability; Magnetic field amplification; PIC simulation

1. Introduction

A significant portion of the universe, comprising interstellar and intergalactic, is occupied by diffuse and high-temperature plasmas. The plasma systems having positive and negative ions with equal charges with equal masses are referred to as pair-plasmas. Among plasma research, these plasma systems have attracted an increasing amount of attention in recent years. The pervasiveness of magnetized electron-positron ($e^- - e^+$) plasmas is found in active galactic nuclei (AGN) [1] and at the core of galaxies [2]. Experiments have also produced nonrelativistic pair plasmas [3], and in tokamaks with multiple MeV runaway electrons, pair production may be possible through collisions with thermal particles. Curiously, recently plasma with fully ionized particles having almost the same absolute charge $(+/-)$ and mass is obtained in the laboratory by generating a large group of fullerene ions. Hence, it is possible to study the properties of pair plasmas without being concerned about mutual annihilation [4]. Along this, the three-component electron-positron-ion (EPI) plasma also became the very interesting plasma due to its existence in various astrophysical environments [5, 6]. The phenomenon by which the cosmic particle is accelerated is still not resolved, which draws the attention of researchers. Fermi postulated that the interplay of magnetic fields and particles in the cosmos is one of the factors for particle acceleration, known as Fermi acceleration [7]. As we know that coulomb interplay among charged particles in the plasma are rare, and the behaviour of the plasma is primarily governed by collective behaviour that engage particles and electromagnetic fields. Therefore, these plasmas are referred to as collisionless plas-

mas. In these plasmas, selective types of "shocks" still take place. These shocks formation generally have very tangled mechanisms that involve various kinetic processes, including electrostatic instabilities, electromagnetic instabilities, and reduction of background magnetic fields. Collisionless shocks observed in extreme astronomical environments cause Fermi acceleration, which results from Weibel instabilities [8, 9] or current filamentation instability. The only method to examine these acceleration processes in an astrophysical setting is by telescopic observation of corresponding radiation spectra. Now the latest field of research in laboratory astrophysics has emerged with the evolution of progressive diagnostic methods with high-power lasers [10]. This gives a new way to mimic the real astrophysical environments in the laboratory, where we can study these systems and can compare the outputs to numerical simulations [11, 12]. For instance, when relativistic intense laser light interacts with solid targets, it results in the acceleration of ions to high energy by different methods, one of the methods being the shock formation [13]. It has also been reported that turbulent magnetic fields are observed in the interaction of hot dense laser targets [14].

The shocks produced within supernova remnants (SNRs) are classified as collisionless shocks. In plasma surroundings the instabilities in relativistic streaming plasmas are pervasive, they play a vital role in magnetic field modification [15] and radiation emission [16] in astrophysical settings like collisionless shocks and relativistic jets. These instabilities are prevalent in laboratory settings involving intense laser and beam-plasma interactions, which are associated with the exploration of laboratory astrophysics [17], in the study of electron [18] and ion [19] transport in high-energy-density and inertial fusion plasmas, and in the development of innovative approaches for compact and luminous gamma-ray sources [20]. Amid the various phenomena occurring in relativistic streaming plasmas, the Weibel instability (known as current filamentation instability) [21] has gained adequate interest as a central mechanism for swiftly enhancing magnetic fields [22]. In the majority of astrophysical and laboratory settings in meager-beam (beam density $\ll$ background density) systems, the magnetic field generated is feeble [23] and constrained to the plasma skin depth on the spatial context [24]. Particles having very high speed this scale is significantly smaller compared to the magnitude of particles gyroradius, so it is remains uncertain how these fields could govern the dynamics of energetic particles.

The nonlinear merging of filaments (small scale structures of charged particle) can gradually enlarge the magnetic field wavelength. However, the present ultrarelativistic particle-in-cell (PIC) simulation implies that saturation is confined to the small spatial domain and low magnetizations $\varepsilon_B \leq 10^{-3}$. The instability's underlying physical process may be explained as follows. When the displacement of electric current takes place formed by the electron streams, comparing one with the other, by some transverse perturbation, the initial displacement current strength is supported by the repulsion of counter-approaching currents. Various numerical simulations have been used to investigate the Weibel instability of electron-positron plasmas in detail. Simulations show that a strong, sub-equipartition magnetic field develops and explodes in counter-streaming electron-positron plasmas as a result of the filamentation instability [25–27]. Moreover, some researchers discovered that even in electron-positron plasmas that are not magnetized, a shock-like structure that is connected to a high magnetic field forms in their simulations with longer computation durations [28–30]. In this study, we probe the magnetic field evolution because of counter-streaming beams of electron-positron (e^-/e^+) pair plasma in the sub-relativistic regime. Our simulations are performed in one dimension (1D) using a complete relativistic PIC code.

2. Theoretical details: The particle-in-cell simulation method

The PIC simulation is a way to model the self-consistently coaction between the electric and magnetic fields with a collision-less kinetic plasma particle [31]. The plasma is considered to be a group of volume elements under consideration as an incompressible phase space fluid. The collective characteristics of the computational particles serve as an approximation to the collective aspects of the corresponding physical plasma species. The Vlasov equation is calculated by the Lorentz equation of motion for each group of volume elements. Each volume element contains a number of particles called super-particles or computational particles (*CP*s) under the constraints of the same charge to mass ratio as the real system. The *CP*s in the simulation zone advance along trajectories guided by the electric (E) and magnetic (B) fields. The charged particles (*CP*s) in the simulation domain move along trajectories influenced by the electric and magnetic fields. The velocity of *CP* at the given position x_{cp} can be defined as v_{cp}. The Maxwell's equations for the fields $E\ (x,\ t)$ and $B\ (x,\ t)$ are given as

$$\nabla \times \mathbf{E} = -\frac{\partial \mathbf{B}}{\partial t}, \quad \nabla \times \mathbf{B} = \mu_0 \varepsilon_0 \frac{\partial \mathbf{E}}{\partial t} + \mu_0 \mathbf{J} \tag{1}$$

$$\nabla \cdot \mathbf{B} = 0, \quad \nabla \cdot \mathbf{E} = \frac{\rho}{\varepsilon_0} \tag{2}$$

and the Lorentz equation of motion

$$\begin{aligned} \frac{d\boldsymbol{p}_{cp}}{dt} &= q_{cp}(\mathbf{E}[x_{cp}] + \boldsymbol{v}_{cp} \times \mathbf{B}[x_{cp}]), \\ \boldsymbol{p}_{cp} &= m_{cp}\boldsymbol{v}_{cp}\Gamma\boldsymbol{v}_{cp}, \quad \frac{dx_{cp}}{dt} = v_{cp} \end{aligned} \tag{3}$$

are solved. The evolution of the electromagnetic fields with time is determined by applying Faraday's law and Ampere's law (Equation (1)). Code compiled Equations (2) $\nabla \cdot \mathbf{E} = \rho/\varepsilon_0$ and $\nabla \cdot \mathbf{B} = 0$ to round off accuracy. Our code utilizes the virtual particle method and ensures the fulfilment of Poisson's equation as a constraint. Equations (3) are employed to update the trajectories of the *CP*s.

Equations (1)– (3) can be rescaled to physical units by using the total plasma frequency $\omega_{pe} = \sqrt{e^2 n_0/m_e\varepsilon_0}$ and skin depth $\lambda_e = c/\omega_{pe}$. In terms of physical units, $\mathbf{E}$ and $\mathbf{B}$ can be normalized as $\boldsymbol{E}_p = \omega_{pe} c m_e \boldsymbol{E}/e$ and $\boldsymbol{B}_p = \omega_{pe} m_e \boldsymbol{B}/e$ respectively, and similarly, the current density $\boldsymbol{J}_p = c n_e e \boldsymbol{J}$.

The simulation time t and position x are given in the units of ω_p and c/ω_p, respectively, and the charge q_{cp} is given in terms of the elementary charge, e. The electric field, magnetic field and current density $\boldsymbol{J}$ are specified on a grid. From the grid to each *CP*, electromagnetic fields are interpolated. The updated momentum of the *CP* can be obtained with these interpolated electromagnetic fields and the Lorentz equation of motion. The new particle position is determined with the help of the old particle position, $\boldsymbol{v}_{cp}$ and time step Δt. The microcurrents are proportional to q_{cp} and $\boldsymbol{v}_{cp}$ which are contributions from each discrete particle, i.e., the *CP*s in our simulations or the particles in real physical plasma systems. They are incorporated from every *CP* back onto the grid, and the current density $\boldsymbol{J}$ can be obtained by integrating over all *CP*s. Now the electromagnetic fields are upgraded from Equation (2), and each step is repeated.

2.1 Simulation details and initial conditions

In this study, we consider two counter-propagating identical beams of electron-positron (e^-/e^+) by using PIC code EPOCH code [32, 33], wherein Dawson [34] provided a general overview of PIC codes. This scenario is pervasive in astrophysical scenarios. It is particularly relevant in the early stages of collisionless shock formation. Our simulations of collisions between electron-positron fireball shells directly relate to internal shocks in gamma ray bursts (GRBs). Periodic boundary conditions are considered for our simulation in all the directions. The one-dimensional simulation box is along the y-direction. The counter-streaming beams are modelled, which move along the x-direction, having initial drift velocities, $\boldsymbol{v}_0 = \pm v_0 x$ with $v_0 = 0.5c$ (with weakly relativistic case). The system has initial Maxwellian particle distribution. Both beams comprise an electron species and a positron species, and all four species possess equal densities. We investigated homogeneous plasma $n(x,\ y) = n_0$, where n_0 is particle number density. In the beginning, all beams exhibit uniform spatial distributions. As mentioned, the simulation box that includes periodic boundary conditions is oriented along the y-direction. The length of the simulation is normalized by ω_{pe}/c, here c is the speed of light in vacuum, and ω_{pe} is electron plasma frequency given by $\omega_{pe} = \sqrt{e^2 n_0/m_e\varepsilon_0}$. Here m_e is the rest mass and e is the charge of the electron. The simulation box has number of cells $N_x = 1$ and $N_y = 1200$ in the x-direction and y-direction, respectively. The length of the simulation box considered is $\Delta x = \Delta y = 0.1c/\omega_{pe}$ and the particle associated with each cell is $N = 32768$. The simulation time step is $\Delta t = 0.05\omega_{pe}^{-1}$. At the start of the simulation, both the electric field (**E**) and magnetic field (**B**) have zero values, i.e., initially, the system is neutral. The overall duration of the simulation is $t_{sim} = 500$.

3. Simulation results

3.1 The field evolution

The filamentation instability, triggered by a plasma flow in the x-direction within a simulation box aligned along the y-direction, initiates the growth of a magnetic field along the z-direction. The chosen velocity vector and the orientation of the simulation box indicate that the particles in both the beams and their micro-currents undergo redistribution solely along the y-axis under the influence of the FI. The neutral plasma, in terms of charge and current, undergoes a transformation into a plasma where $J_x(y) \neq 0$. As per Equation (1), an increase in $J_x(y)$ only affects the $E_x(y)$ and $B_z(y)$ components of the electric and magnetic fields. This occurs because the gradients in the x and z-directions become zero in the one-dimensional geometry. As stated by Ampere's law, $dB_z/dy = J_x + \partial E_x/\partial t$, the increasing net current $J_x(y)$ will give rise to the growth of E_x. The redistribution of particles causes the formation of a space charge, which in turn generates an electric field $E_y(y)$.

Figure 1 depicts ε_B and ε_E in the temporal history of electric and magnetic field energy. The energy density of the magnetic component B_z, denoted as ε_{Bz}, becomes dominant and reaches a few percent of the total energy, consistent with previous simulations. The energy density ε_{Ex} cannot be ascribed to the quasilinear electron instability because ε_{Ex} should have twice the exponential growth rate of ε_{Bz} till $t \sim 8\omega_{pe}^{-1}$. The electric field component ε_{EY} grows at the same rate as ε_{Bz}. The energy densities ε_{Bz} and ε_{EY} grow linearly with time in the range $1 < t < 10$ and then saturates for the rest of the time. As we can see from the figure, magnetic field energy grows exponentially in linear regime as seen by the linear theory, and then, after the initial saturation the further disturbances are found because of the irregularities in the structure of trapped particles [13]. by observing the energy history of a one-dimensional problem involving two beams, which was analyzed using a brief computational grid. At the end, the steady-state distribution occurs. The electric field energy is low compared to the magnetic field [14]. The energy increases with coalescing as time increases. The 10% of the energy is converted to magnetic energy, but in the case of instability in electrostatic two-beam systems, only 2 to 3% is converted into magnetic field energy, and this energy decreases if there is further coalescing. The difference is due to the fact that because energy should be conserved between magnetic energy and kinetic energy allied with particle trapping; here both degrees of freedom acquire energy by a third, the x-component of the

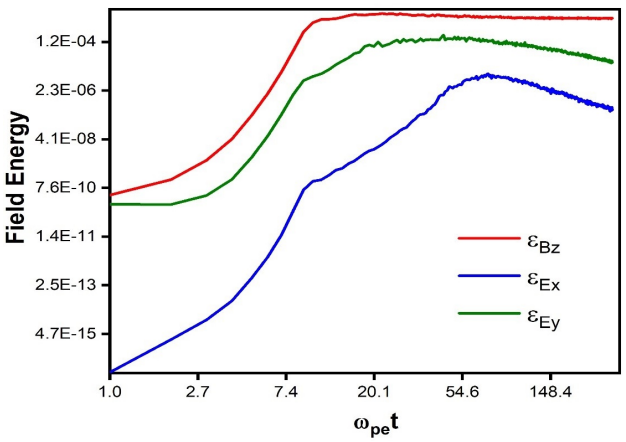

Figure 1. Temporal evolution of the electromagnetic energies of $E_x(i.e.\ \varepsilon_{Ex})$, $E_y(i.e.\ \varepsilon_{Ey})$ and $B_z(i.e.\ \varepsilon_{Bz})$ on logarithmic scale for counter-streaming plasma flows.

velocity of particles.

The field components B_z, E_y start to saturate near $t \sim 8\omega_{pe}^{-1}$, then $B_z(y,\, t)$ almost remains practically stationary while $E_x(y,\, t)$ starts damped after $t \sim 50\omega_{pe}^{-1}$. The E_y shows the pattern as the B_z after the saturation, which is understood from the magnetic pressure gradient as

$$-eE_y = \frac{1}{n_e \mu_0} B_z \frac{dB_z}{dy} \tag{4}$$

3.2 The spatial profile of magnetic field

Figure 2 shows the time sequence of magnetic $B_z(y)$ profile obtained from one-dimensional simulation. With the above temporal evolution of magnetic field energy, we can observe the magnetic perturbations. These perturbations are observed at six different simulation times. These plots of $B_z(y)$ are plotted in the terms of $(4\pi n_0 mc^2)^{1/2}$ with n_0 and m is the initial particle density and mass of the particle, respectively. The simulation shown below starts with the number of wavelengths, and other runs have different sets. The particle trapping structure starts developing from its initial time and is fully developed at simulation time $t = 30\omega_{pe}^{-1}$. The profile of $B_z(y)$ apparent to fit to the particle-trapping structures. The simulations at other times $t = 100,\, 500\omega_{pe}^{-1}$ depict the further coalescing of the trapping zones. Figure 2 (a) is corresponding to simulation time $t \sim 1\omega_{pe}^{-1}$ i.e., at the initial time, the order of the magnetic field is 14, and at simulation time, $t \sim 8\omega_{pe}^{-1}$ the magnitude increases and becomes of an order of 400 and goes on increasing for a time and becomes 600, i.e., constant for the latter simulation time. According to these observations, we can say that

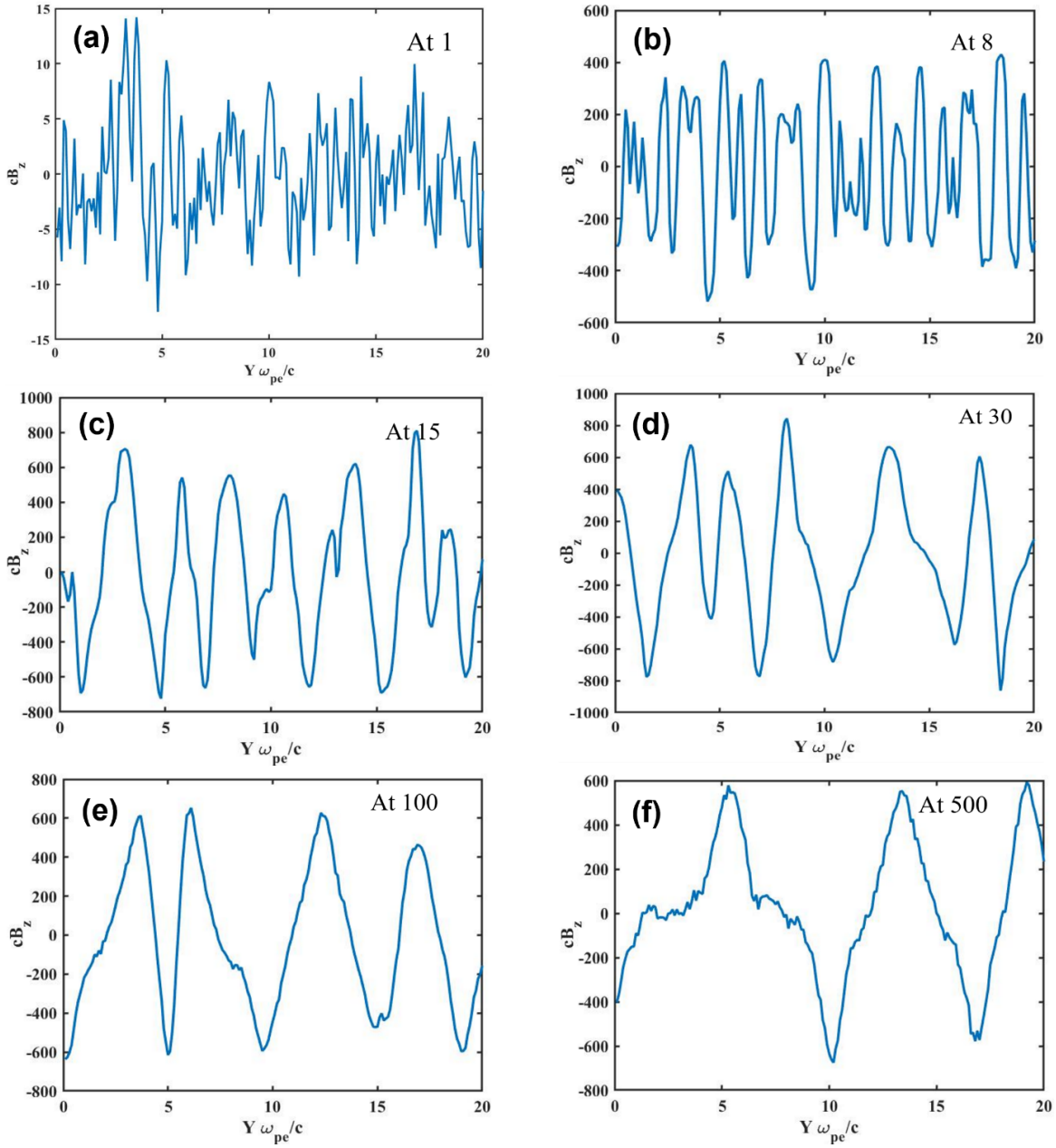

Figure 2. Time evolution of the magnetic field profile for counter-streaming plasma flows. Figures (a), (b), (c), (d), (e), and (f) show magnetic perturbations at simulation time 5, 8, 15, 30, 100, and 500, respectively. The y-axis has the unit of V/m.

at first, the magnetic field magnitude is very small. The magnitude of the magnetic field increases with time and continues to increase as time passes.
The magnetic field is oscillatory and directly linked to the phase space distribution because of the charge particle distribution. This distribution of charges generates the current density and results in the magnetic field. The wavelength of the magnetic field profile generated at different simulation times is interconnected to the phase space distribution at the corresponding time. A similar trend is observed in the time evolution of the magnetic field, i.e., as time passes, the amplitude of the magnetic field energy also increases and becomes almost constant for the rest of time. Hence these results are in agreement with the time evolution of the magnetic field.

3.3 Phase-space distribution

In order to gain additional information, one can examine particle phase space distributions. We focused on the electron-positron phase space distribution $f(y, v_x)$ because this is the plane containing the plasma structures that develop due to the instability. The particles of beam one move along the y-direction. One of the noticeable characteristics of the phase space plots for the simulation particles depicted below is the occurrence of magnetic trapping. This phenomenon can be explained as. The distribution at six different computational times is shown in Figure 3. Since both the beams will have the same distribution, we have shown only one beam. Initially, the beam is almost spatially homogeneous. During the initial linear growth regime, $1 < tw_p < 8$ of the instability, the particles are distributed along the y-direction, as shown in Figure 3 (a). The instability produces a distribution that moves in a zig-zag pattern, and this movement causes the electric field to grow through its currents. Still, the phase space distortion is weak, and the evolution of E_y is not crucial. The magnetic field is still expanding enormously at this point. The forces resulting from E_y and $v_{cp}B_z$ are currently insufficient to alter the particle paths. The particles exhibit only thermal motion in the y-direction until robust electromagnetic fields are created. When the electromagnetic fields reach a substantial level after $t_{\omega p} = 8$, they force the particles to move closer together in the y-direction, creating a structure with layers in the distribution of the phase space. As time passes, the complexity of the phase space distribution becomes more pronounced. After the saturation of instability in Figure 1, the particles start their separation from phase-space spatial distribution. The phase space looks like stationary in time at the end of simulation time. The mechanism behind the density accumulation and the formation of the zig-zag distribution can be explained as follows. Particles that possess a positive x-component of momentum and a positive z-component of the magnetic field, i.e., $p_x > 0$, E_y, $B_z < 0$, experience a particular effect. In this case, the electric field accelerates the electrons away from the break in the direction of increasing y, while the positrons are accelerated along the y-direction.
The field component E_x enhances the distribution of particles from its initial distribution in the x-direction. The magnetic field profile and phase space distribution has direct resemblance. The plots at time points 30, 100, and 500 depict the gradual merging of trapping regions, resulting in six, four, and three regions, respectively. This pattern closely resembles the coalescing observed in the electrostatic scenario with two equal beams, as documented in [35] and previously observed in [36].

3.4 Dominant component of electric and magnetic fields

We have investigated and quantified the relationship between the electric and magnetic fields, as well as their impact on the trajectories of particles. There exists a consistent correlation between both the fields. Figure 4 shows that the B_z and E_y field components have a direct connection with the phase space distribution. Damped E_y is shifted by the phase relative to B_z when the FI saturates. It is revealed from Figure 5 when $E_x \neq 0$ implies that $dB_z/dy \neq 0$ or $B_z \neq 0$, this leads to a finite magnitude of the magnetic pressure in the gradient. The current density calculated from the equation $\boldsymbol{J}(\boldsymbol{x}, t) = q\int_{-\infty}^{+\infty} \boldsymbol{v} f(x, \boldsymbol{v}, t) d\boldsymbol{v}$ is depicted in Figure 5 (b). Current experienced a force caused by the magnetic pressure gradient is $\boldsymbol{J} \times \boldsymbol{B} = -\boldsymbol{\nabla} B^2/2$. Only the B_z is growing under the considered geometry and ∂_y is only viable spatial derivative, The force exerted on the particles by the magnetic pressure gradient force (MPGF) can only be transmitted through the presence of an electric field force in the y-direction. So, the above equation is simplified to $J_x B_z = B_z dB_z/dy$. The strength of B_z is strong for simulation time $t > 8$ and $dB_z/dy \neq 0$. The right-hand side of the MPGF in the above equation is not equal to zero, hence this is the cause of the particle $\boldsymbol{E} \times \boldsymbol{B}$ force pushes the particles along y-direction. The charge density fluctuations are associated with Figure 5 (a) at the end of the simulation. It appeared after the saturation of the instability, i.e., the acceleration. The electrostatic instability results in the electrostatic waves. Hence, this electrostatic instability results in the growth of E_y between $7 < t < 500$.
We can understand one potential cause of this electrostatic instability. The electrons of beam one has a velocity with $-v_b x$, whereas the positrons with $v_b x$. The currents generated by these streams have the same sign, and the MPGF accelerates both the species along the y-direction. As much as the density of positrons and electrons is constant throughout, the growth of E_x does not occur, since $J_x = 0$ in $\partial_t E_x + J_x = 0$. Hence, MPGF is not the reason of E_x – field. Nonetheless, the random fluctuations in the charge density (Figure 5 (a)) because of the finite number of the *CP*s insinuate that the MPGF pushes locally (on the length scale of Debye length) with different numbers of electrons and positrons, which imply $J_x \neq 0$. An electric field evolves aiming to restore the balance of charge neutrality. The MPGF combines with these fluctuations when the force gradient is high (similar to the length scale of fluctuations) and when the oscillations of force resonate with the characteristic frequency of the fluctuations. After the simulation time $t > 20$ the E_x experiences a deceleration in growth rate or becomes almost constant because there may be more reduction in the intense and shorter oscillations of MPGF $B_z dB_z/dy$. The initial zig-zag distribution is modified and becomes stationary phase space distribution. On the linear

and 10-logarithmic density scales, the width of the distribution in p_x has the same structure along the y-direction. Recently we have published an article [12], in which we used two-dimensional PIC simulation code and studied the magnetic field amplification for an initially unmagnetized, spatially uniform, counterstreaming electron–positron plasma flow and compared this with nonuniform flow case. Here the magnetic field energy amplification shows that in the beginning the magnetic field grows exponentially and then decays with further saturation but for the inhomogeneous case we have a second peak in the magnetic field energy after its first saturation. This type of behaviour is directly connected to the density perturbation in upstream plasma flow, and temperature anisotropy is the reason for this amplification of the magnetic field in the inhomogeneous case. This type of particular density distribution is common in Gamma-ray bursts. However, in the present study, we considered homogeneous plasma distribution case and realized that the magnetic field energy initially shows the linear behaviour and then saturates for the rest of the simulation time due to kinetic effects. The phase space analysis indicates the filamentation instability by coalescing of plasma particles, and spatial evolution of magnetic field is connected to the phase space distribution. These types of simulations can present the important information related to the magnetic field structures, strength and scale size. These

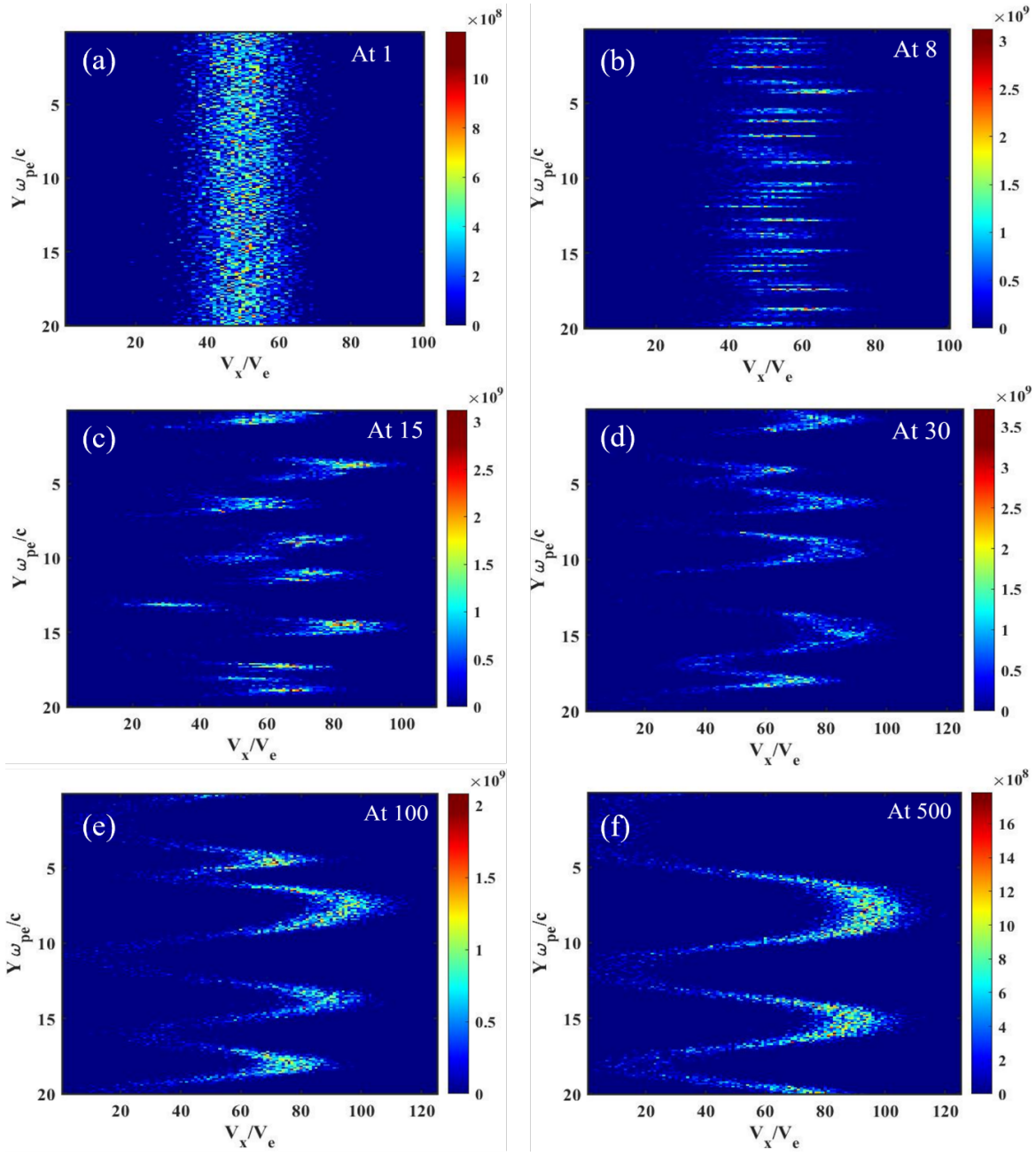

Figure 3. Shows the phase space densities of the distribution function of $f(y,\ v_x)$ of beam one in the units of computational particles: panel (a) depicts the initial time distribution, panel (b) at simulation time $t = 8$, panel (c) at simulation time $t = 15$, (c) at simulation time $t = 30$, (c) at simulation time $t = 100$, and at the end (d) at simulation time $t = 500$.

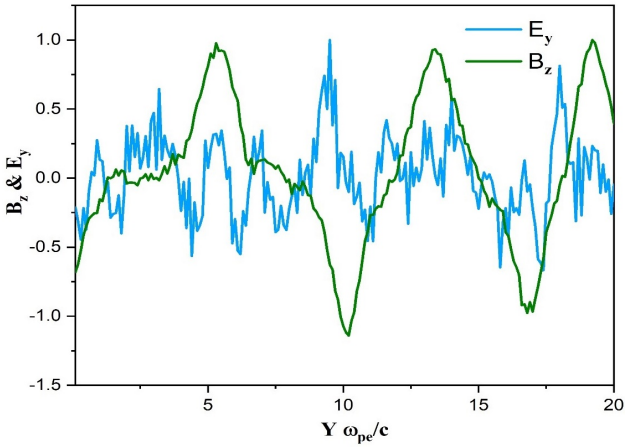

Figure 4. Shows the dominant component of the magnetic field and electric field. The panel shows the B_z–component of the magnetic field (green line) and the E_x-component of electric field (blue line) at the simulation time $t \approx 500$. The y-axis has the unit of V/m.

structures are developed due to nonthermal particle distributions dominant in astrophysical flows and may offer an insight related to synchrotron radiation.

4. Discussion and conclusion

This paper examines the FI phenomenon caused by the interaction of two opposing beams, each composed of both electrons and positrons. Our analysis is restricted to an electron-positron plasma with sub-relativistic and unmagnetized plasma. Considering the beams to be spatially uniform, we have performed one-dimensional simulations with a simulation box along the y-direction having a large number of particles along this side, which restrain the growth of filaments after a certain size. The two beams travelling in the opposite directions (x) with a speed of $0.5c$ is enough to exclude notable sub-relativistic effects. Our purpose is to understand the kinematics of a filament pair generated because of the counter-streaming beams of electron-positron as inspired by those used in [37]. This instability reorganizes charge particles in space and forms current filaments. The currents and densities accumulate due to both the species. The MPGF accelerates both the species along a direction because of the symmetry between these species within a filament. The simulation demonstrated that E_y would speed up the electrons as they moved out from the centre of the filament. The inclusion of positrons in this simulation work eliminates this repulsion. Electron-positron species can achieve larger charge and current densities compared to electron-only beams and have wider filament spacing. The magnetic field can achieve larger spatial variations. The growth of a magnetic field up to an amplitude is posed by magnetic trapping.

As anticipated, solely the magnetic energy density's z-component has been amplified. Following an initial stage of exponential growth in the B_z field, the wave has reached its maximum. The evolution of B_z has resulted from the transformation of the particle velocity distribution, which was initially uniform in space, into a zig-zag distribution in phase space. This distribution exhibits piecewise linear variation in mean speed along the x-axis, which is dependent on y. In the majority of the simulation box, the initial value of $J_y = 0$ has been changed to $J_y \neq 0$. The one-dimensional simulation shows the evolution of electrostatic E_y component. The 1D PIC simulation gives insight into the correlation between the particle's phase space structures and the fields, and the nonlinear stage of the instability leads to the development of charge density oscillations, which can be resolved using it. The complexity of this zig-zag distribution is explained in more detail. They correspond to the positions at which the change with y of the mean momentum along x reverses its sign.

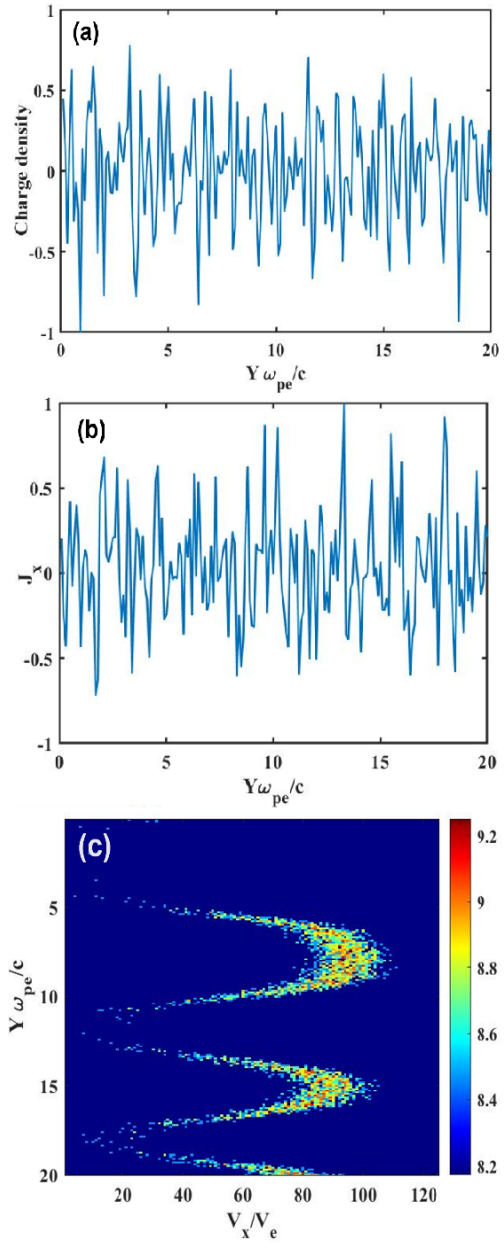

Figure 5. Simulation at end time $t \approx 500$; panel (a) shows the charge density, and panel (b) shows the x-component of charge density. Panel (c) the logarithmic particle phase space density, expressed in units of charged particles (CPs), is represented on a 10-logarithmic scale.

The Weibel instability cannot always be justified by solely focusing on magnetic forces and ignoring electric forces. With the present ability to achieve high phase space resolution in PIC simulations, it has been uncovered that in the 1D simulation, the filament size grows not by the merging of filaments, as prevented by the 1D geometry, but through the widening of filaments caused by the overlapping of phase space layers. The link between the magnetic and electric fields generated by the instability is similar to that observed in the filamentation instability, which arises from the interaction of counter-propagating electron-positron beams. The phase space distribution in the 1D simulation initially displayed intricate features that gradually transformed into a thermalized distribution characterized by a predominant zig-zag pattern. These simulations could offer valuable information regarding the magnetic field structures' field strength and scale size, which are developed because of nonthermal particle distributions leading to the emergence of astrophysical flows, and to what degree these structures might contribute to the observed synchrotron radiation.

Acknowledgements

Rakesh Kumar thanks the High-Performance Computing (HPC) cluster at IIT Delhi for enabling Particle-in-Cell simulations. The authors also extend gratitude to the developers of EPOCH codes for supplying the necessary diagnostics upon request. Furthermore, Rakesh Kumar acknowledges the Council of Scientific and Industrial Research (CSIR), Government of India, for providing financial support through Grant Reference Number 09/086(1369)/2018-EMR-1.

Authors Contributions
All the authors have participated sufficiently in the intellectual content, conception and design of this work or the analysis and interpretation of the data (when applicable), as well as the writing of the manuscript.

Availability of Data and Materials
All the data generated is included in the manuscript.

Conflict of Interests
The authors declare that they have no known competing financial interests or personal relationships that could have appeared to influence the work reported in this paper.

References

[1] M. C. Begelman, R. D. Blandford, and M. J. Rees. "Theory of extragalactic radio sources.". *Reviews of Modern Physics*, **56**:255, 1984. DOI: https://doi.org/10.1103/RevModPhys.56.255.

[2] D. J. Forrest, M. L. Burns, A. K. Harding, and R. Ramaty. "Positron-electron pairs in astrophysics.". *AIP Conf. Proc.*, **101**, 1983.

[3] R. G. Greaves, M. D. Tinkle, and C. M. Surko. "Creation and uses of positron plasmas.". *Physics of Plasmas*, **1**:1439–1446, 1994. DOI: https://doi.org/10.1063/1.870693.

[4] W. Oohara and R. Hatakeyama. "Pair-ion plasma generation using fullerenes.". *Physical Review Letters*, **91**:205005, 2003. DOI: https://doi.org/10.1103/PhysRevLett.91.205005.

[5] S. Lashgarinezhad, A. H. Sari, and D. Dorranian. "Effects of nonthermal electrons and positrons on the characteristics of ion-acoustic cnoidal wave in electron-positron-ion plasma. ". *Chaos, Solitons & Fractals*, **103**:261–270, 2017. DOI: https://doi.org/10.1013/j.chaos.2017.06.010.

[6] F. Farhadkiyaei and D. Dorranian. "Nonlinear ion-acoustic cnoidal wave in electron-positron-ion plasma with nonextensive electrons. ". *Contributions to Plasma Physics*, **58**:42–55, 2018. DOI: https://doi.org/10.1002/ctpp.201600076.

[7] E. Fermi. "On the origin of the cosmic radiation. ". *Physical Review*, **75**:1169, 1949. DOI: https://doi.org/10.1103/physRev.75.1169.

[8] E. S. Weibel. "Spontaneously growing transverse waves in a plasma due to an anisotropic velocity distribution. ". *Physical Review Letters*, **2**:83, 1959. DOI: https://doi.org/10.1103/PhysRevLett.2.83.

[9] R. Z. Sagdeev. "The 1976 Oppenheimer lectures: Critical problems in plasma astrophysics. II. Singular layers and reconnection.". *Reviews of Modern Physics*, **51**:11, 1979. DOI: https://doi.org/10.1103/RevModPhys.51.1.

[10] P. Maine, D. Strickland, P. Bado, M. Pessot, and G. Mourou. "Generation of ultrahigh peak power pulses by chirped pulse amplification.". *IEEE Journal of Quantum Electronics*, **24**:398–403, 1988. DOI: https://doi.org/10.1109/3.137.

[11] J. M. Dawson. "Particle simulation of plasmas.". *Reviews of Modern Physics*, **55**:403, 1983. DOI: https://doi.org/10.1103/RevModPhys.55.403.

[12] R. Kumar, H. K. Malik, and S. Kumar. "Study of magnetic field evolution by Weibel instability in counter-streaming electron–positron plasma flows.". *J Astrophys Astron*, **45**:13, 2024. DOI: https://doi.org/10.1007/s12036-024-10001-3.

[13] M. Q. He, Q. L. Dong, Z. M. Sheng, S. M. Weng, M. Chen, H. C. Wu, and J. Zhang. "Acceleration dynamics of ions in shocks and solitary waves driven by intense laser pulses.". *Physical Review E*, **76**:035402, 2007. DOI: https://doi.org/10.1103/PhysRevE.76.035402.

[14] S. Mondal, V. Narayanan, W. J. Ding, A. D. Lad, B. Hao, S. Ahmad, and G. R. Kumar. "Direct observation of turbulent magnetic fields in hot, dense laser produced plasmas. ". *National Academy of Sciences*, **109**:8011–8015, 2012. DOI: https://doi.org/10.1073/pnas.1200753109.

[15] A. E. Broderick, P. Chang, and C. Pfrommer. "The cosmological impact of luminous TeV blazars. I. Implications of plasma instabilities for the intergalactic magnetic field and extragalactic gamma-ray background. ". *The Astrophysical Journal*, **752**:22, 2012. DOI: https://doi.org/10.1088/0004-637X/752/1/22.

[16] A. Gruzinov and E. Waxman. "Gamma-ray burst afterglow: polarization and analytic light curves.". *The Astrophysical Journal*, **511**:852, 1999. DOI: https://doi.org/10.1086/306720.

[17] E. Boella, K. Schoeffler, N. Shukla, M. E. Innocenti, G. Lapenta, R. Fonseca, and L. O. Silva. "Interaction between electrostatic collisionless shocks generates strong magnetic fields. ". *New Journal of Physics*, **24**:063016, 2022. DOI: https://doi.org/10.1088/1367-2630/ac6ef1.

[18] L. O. Silva, R. A. Fonseca, J. W. Tonge, W. B. Mori, and J. M. Dawson. "On the role of the purely transverse Weibel instability in fast ignitor scenarios. ". *Physics of Plasmas*, **9**:2458–2461, 2002. DOI: https://doi.org/10.1063/1.1476004.

[19] S. Göde, C. Rödel, K. Zeil, R. Mishra, M. Gauthier, F. E. Brack, and F. Fiuza. "Relativistic electron streaming instabilities modulate proton beams accelerated in laser-plasma interactions. ". *Physical Review Letters*, **118**:194801, 2017. DOI: https://doi.org/10.1103/PhysRevLett.118.194801.

[20] A. Benedetti, M. Tamburini, and C. H. Keitel. "Giant collimated gamma-ray flashes.". *Nature Photonics*, **12**: 319–323, 2018. DOI: https://doi.org/10.1038/s41566-018-0139-y.

[21] B. D. Fried. "Mechanism for instability of transverse plasma waves.". *Physics of Fluids*, **2**:337, 1959. DOI: https://doi.org/10.1063/1.1705933.

[22] A. Grassi, M. Grech, F. Amiranoff, F. Pegoraro, A. Macchi, and C. Riconda. "Electron Weibel instability in relativistic counterstreaming plasmas with flow-aligned external magnetic fields.". *Physical Review E*, **95**:023203, 2017. DOI: https://doi.org/10.1103/PhysRevE.95.023203.

[23] F. Califano, T. Cecchi, and C. Chiuderi. "Nonlinear kinetic regime of the Weibel instability in an electron–ion plasma. ". *Physics of Plasmas*, **9**:451–457, 2002. DOI: https://doi.org/10.1063/1.1435001.

[24] R. C. Davidson, D. A. Hammer, I. Haber, and C. E. Wagner. "Nonlinear development of electromagnetic instabilities in anisotropic plasmas. ". *The Physics of Fluids*, **15**:317–333, 1972. DOI: https://doi.org/10.1063/1.1693910.

[25] Y. Kazimura, J. I. Sakai, T. Neubert, and S. V. Bulanov. "Generation of a small-scale quasi-static magnetic field and fast particles during the collision of electron-positron plasma clouds. ". *The Astrophysical Journal*, **498**:183, 1983. DOI: https://doi.org/10.1086/311316.

[26] L. O. Silva, R. A. Fonseca, J. W. Tonge, J. M. Dawson, W. B. Mori, and M. V. Medvedev. "Interpenetrating plasma shells: near-equipartition magnetic field generation and nonthermal particle acceleration. ". *The Astrophysical Journal*, **596**:121, 2003. DOI: https://doi.org/10.1086/379156.

[27] K. I. Nishikawa, P. Hardee, G. Richardson, R. Preece, H. Sol, and G. J. Fishman. "Particle acceleration and magnetic field generation in electron-positron relativistic shocks.". *The Astrophysical Journal*, **622**:927, 2005. DOI: https://doi.org/10.1086/428394.

[28] A. Gruzinov. "Strong relativistic collisionless shock.". , 2001. DOI: https://doi.org/10.48550/arXiv.astro-ph/0111321.

[29] T. Haruki and J. I. Sakai. "Generation of magnetic field and electrostatic shock wave driven by counterstreaming pair plasmas. ". *Physics of Plasmas*, **10**:392–397, 2003. DOI: https://doi.org/10.1063/1.1540095.

[30] T. Bulik, B. Rudak, and G. Madejski. "Astrophysical sources of high energy particles and radiation. ". *AIP Conference Proceedings*, **801**, 2005.

[31] R. Bühler and R. Blandford. "The surprising Crab pulsar and its nebula: a review.". *Reports on Progress in Physics*, **77**:066901, 2014. DOI: https://doi.org/10.1088/0034-4885/77/6/066901.

[32] T. D. Arber, K. Bennett, C. S. Brady, A. Lawrence-Douglas, M. G. Ramsay, N. J. Sircombe, and C. P. Ridgers. "Contemporary particle-in-cell approach to laser-plasma modelling.". *Plasma Physics and Controlled Fusion*, **57**:113001, 2015. DOI: https://doi.org/10.1088/0741-3335/57/11/113001.

[33] C. K. Birdsall and A. B. Langdon. "Plasma physics via computer simulation. ". *CRC Press*, , 2004. DOI: https://doi.org/10.1201/9781315275048.

[34] J. M. Dawson. "Particle simulation of plasmas. ". *Reviews of Modern Physics*, **55**:403, 1983. DOI: https://doi.org/10.1103/RevModPhys.55.403.

[35] R. L. Morse and C. W. Nielson. "One-, two-, and three-dimensional numerical simulation of two-beam plasmas. ". *Physical Review Letters*, **23**:1087, 1969. DOI: https://doi.org/10.1103/PhysRevLett.23.1087.

[36] H. L. Berk and K. V. Roberts. "Nonlinear study of Vlasov's equation for a special class of distribution functions. ". *Physics of Fluids*, **10**:1595–1597, 1967. DOI: https://doi.org/10.1063/1.1762331.

[37] A. Stockem, M. E. Dieckmann, and R. Schlickeiser. "PIC simulations of the thermal anisotropy-driven Weibel instability: field growth and phase space evolution upon saturation.". *Plasma Physics and Controlled Fusion*, **51**:075014, 2009. DOI: https://doi.org/10.1088/0741-3335/51/7/075014.